https://doi.org/10.5194/essd-2026-831
Preprint. Discussion started: 9 November 2026
© Author(s) 2026. CC BY 4.0 License.



Open Access Earth System Science Data Discussions

High precision atmospheric GHG measurements for the Orinoco region: The Villavicencio Tower (VLO)

Stijn Hantson[1,2]*, Santiago Botía[2,]*, Miguel Ángel Navarro-Ramírez[3], Diego Pardo-Buitrago[3], João Fernandes Amaral[1], Shrutika Wagh[2], Miguel Ángel Ramírez-Niño[3], Anghy Gutierrez-Rincon[1], Mauricio Salamanca[1], Armin Jordan[2], Steffen Knabe[2], Tarek El Madany[2], Karl Kuebler[2], Heiko Moossen[2], Michael Rothe[2], Christian Rödenbeck[2], Sönke Zaehle[2], Carlos Sierra[2]

[1] Escuela de Ciencias e Ingeniería, Universidad del Rosario, Bogotá, Colombia
[2] Max Planck Institute for Biogeochemistry, Jena, Germany
[3] Universidad de los Llanos, Villavicencio, Colombia

* These authors contributed equally

Contact authors:
Stijn Hantson: stijn.hantson@urosario.edu.co, shantson@bgc-jena.mpg.de
Santiago Botía: sbotia@bgc-jena.mpg.de

Abstract

Understanding the dynamics of natural and anthropogenic sources and sinks of greenhouse gases (GHG) is key to projecting anthropogenic climate change and detecting potential climate-carbon feedbacks. While our understanding of the sources and sinks has increased considerably over the past decades, much of the progress has focused on extratropical ecosystems, leaving large parts of the tropics understudied. Tropical ecosystems are assumed to be important carbon sinks and significant sources of methane, but much of the temporal and spatial heterogeneity and trends are still poorly understood. Observational efforts have largely concentrated on key tropical regions such as the Amazon Basin, whereas other tropical areas remain sparsely monitored with in-situ measurements. In particular, northern South America—despite being identified by bottom-up and top-down models as a significant contributor to global GHG budgets—currently lacks atmospheric observations to evaluate these estimates or resolve their spatial and temporal variability. To address this observational gap, here we present the establishment of the Villavicencio Tower (VLO) for atmospheric GHG measurements to provide additional constraints on GHG emission estimates across northern South America. This 26 m tower is located within the Orinoco lowlands, close to the Andean foothills in Colombia. Due to the predominantly easterly winds in the region, the footprint covers the Orinoco basin and the northern Amazon. Weekly duplicated flask measurements are taken, and laboratory analysis of trace gases (CO_2, CH_4, CO, N_2O, SF_6, H_2) and the stable isotope composition of CO_2 (^{13}C and ^{18}O) and CH_4 (^{13}C and ^{2}H) are performed, as well as O_2/N_2 and Ar/N_2. The tower started operating on 20 June 2023 and here we present the first 21 months of data. Time series of all measurements are presented as well as a discussion regarding uncertainties. These measurements will allow for improved estimates of GHG emissions across northern South America and to detect long-range transport across the Amazon to the Orinoco river basin.

https://doi.org/10.5194/essd-2026-831
Preprint. Discussion started: 9 November 2026
© Author(s) 2026. CC BY 4.0 License.



Open Access Earth System Science Data Discussions

1. Introduction

Atmospheric greenhouse gas (GHG) mixing ratios are increasing year after year, driving anthropogenic climate warming. The main GHG gases driving this anthropogenic climate change are CO_2, CH_4 and N_2O, in decreasing order of importance. Over the past few decades, our understanding of the drivers, sources, and sinks of these gases has advanced considerably (Arias et al., 2021). These advances have allowed the generation of functional processed-based models that are able to estimate global budgets for the main GHGs (Friedlingstein et al., 2025; Saunois et al., 2025; Tian et al., 2024). In parallel, improvements in atmospheric inversion methods (Houweling et al., 2017), together with the increasing availability of globally distributed atmospheric observations and remotely sensed products, have helped constrain these process-based global estimates (Ciais et al., 2013; Peylin et al., 2013).

The annually updated global CO_2 budget estimates generated by the Global Carbon Budget (Friedlingstein et al., 2025) provide annual assessments of atmospheric CO_2 growth rates and their underlying drivers. Similar projects have produced budgets for methane (Saunois et al., 2025) and nitrous oxide (Tian et al., 2024). These studies have clarified the importance of distinguishing between anthropogenic and natural sources, highlighting the dominant role of fossil fuel emissions in driving CO_2 increases, the substantial contribution of agriculture and wetlands to methane emissions, and the key influence of agricultural practices on nitrous oxide fluxes. Together, these coordinated efforts have improved our understanding of the global greenhouse gas budget and reduced uncertainties in source attribution.

Despite these advances, substantial uncertainties remain regarding the magnitude, dynamics, and spatial distribution of greenhouse gas (GHG) sources and sinks (Canadell et al., 2021). Much of the progress to date has focused on extratropical regions, while research in the tropics has largely concentrated on a few key areas, such as the Amazon rainforest, leaving many tropical regions understudied (Watts et al., 2026). This imbalance leads to large uncertainties in these regions, both in process-based global models and in atmospheric inversion studies, where sparse observational networks limit representation. As a result, tropical GHG fluxes remain comparatively poorly constrained although some of these have been recognized as key source regions at a global scale (Feng et al., 2022; Gentine et al., 2019).

One such region is the Orinoco basin in northern South America (Fernandes Amaral et al., 2026). This region is covered by natural savannas (the Llanos) and tropical rainforest. Part of these savannas present biomass-burning during the dry season (December-April) but also flooding during the wet season (May-November), which, together with the other wetland systems in South America (e.g. Pantanal (Gloor et al., 2021), and Llanos de Moxos (France et al., 2022) make it an important source of methane at a global scale. Furthermore, savanna management has traditionally been based on cattle ranching, but the region is currently undergoing rapid agricultural transformation driven by the expansion of oil palm plantations and rice cultivation. Due to its remoteness and political instability, limited field data is available, leaving us in the dark on the importance of this area for global GHG fluxes and how it is responding to ongoing climate change and socio-economical dynamics (Fernandes Amaral et al., 2026).

One approach to monitoring such regions is through the use of remotely sensed data (He et al., 2026). Over the past decades, substantial advances have been made in estimating atmospheric column-averaged mixing ratios of CO_2 and CH_4 from satellite observations (Buchwitz et al., 2015).

https://doi.org/10.5194/essd-2026-831
Preprint. Discussion started: 9 November 2026
© Author(s) 2026. CC BY 4.0 License.



Open Access Earth System Science Data Discussions

These datasets enable monitoring at the global and regional scale, helping to fill observational gaps in regions where in situ measurements are sparse or absent. However, satellite-derived products are subject to their own uncertainties and biases (Frankenberg et al., 2024) and therefore require validation against ground-based observations. The limited availability of such measurements across large parts of the tropics increases the uncertainty associated with these estimates in these key tropical regions (Hancock et al., 2025, 2026).

An alternative approach for monitoring greenhouse gases (GHGs) is through high-precision atmospheric measurements at the surface. Temporal variations in atmospheric mole fractions, as well as differences among monitoring stations, can be used to infer the spatial dynamics and trends of regional GHG fluxes, typically in combination with atmospheric transport and inverse modeling, which relate observational gradients to surface fluxes. An important advantage of atmospheric flask monitoring over remotely-sensed columns is the ability to obtain stable and radioactive isotopologues on CO_2 and CH_4 (Heimann et al., 2022; Sierra et al., 2025), which are crucial for source attribution and process understanding. Although global atmospheric observation networks have been established in the last decades (Schuldt et al., 2025), these stations are concentrated in extratropical regions, with a focus on monitoring background air and with relatively limited coverage across the tropics. This sparse coverage partly reflects the logistical and infrastructural challenges associated with establishing and maintaining long-term atmospheric monitoring stations in remote tropical environments. One notable exception is the Amazon Tall Tower Observatory (ATTO), which was established to monitor atmospheric composition and ecosystem–atmosphere interactions across a large portion of the Amazon rainforest (Andreae et al., 2015). In addition, aircraft-based vertical profile measurements have been collected over the past decades in several parts of the Amazon Basin (Gatti et al., 2021, 2023), resulting in comparatively good observational coverage for this region. However, the prevailing easterly trade winds largely constrain the source regions represented by these measurements to central and eastern Amazonia, leaving the Orinoco plains and the northern Amazon poorly monitored (Botía et al., 2025).

Considering the limited availability of field data on GHG fluxes and the fact that no atmospheric monitoring station adequately covers northern South America, we established the Villavicencio Tower (VLO) in the Orinoco floodplains near the Andean foothills, outside the city of Villavicencio, Colombia. The main objective of the VLO tower is to produce a record of high precision atmospheric measurements of greenhouse gases and their isotopic composition for the understudied region of the Orinoco Llanos. In addition, we aim at integrating the results of this monitoring program into a larger network of global atmospheric observations that are currently used for atmospheric inversion studies and for producing global budgets of GHGs. Here, we describe the characteristics of the tower, the sampling and analytical procedures, its seasonal footprint, and present the time series from the first 21 months of data collection. We also discuss data limitations and tower characteristics that should be taken into account for the appropriate use of the collected data.

2. Methods

2.1 Tower and flask measurement description

Measurements are taken from a 26 m high tower (4°04’23.75’’N; 73°35’05.31’’W), located within the Barcelona Campus of Universidad de Los Llanos (Unillanos), approximately 9 km south-west of the city of Villavicencio, Colombia. Advantage was taken from an existing 20 m high structure, on top of which a 6 m high tower was constructed (see Figure S1 for a photo of the tower). The tower

https://doi.org/10.5194/essd-2026-831
Preprint. Discussion started: 9 November 2026
© Author(s) 2026. CC BY 4.0 License.



is approx. 1750 km away from the nearest other atmospheric monitoring station at ATTO and approx. 1850 km away from the background NOAA station of Ragged Point Barbados (Figure 1). Due to the predominantly easterly winds, the atmospheric measurements of Barbados and Ascension Island (NOAA stations) should be informative regarding the background atmospheric conditions reaching the continent.

Since 20 June 2023, weekly atmospheric flask samples have been collected at the tower site using a manual sampler (Figure S2 (Heimann et al., 2022)). The inlet is located at the top of the tower (26 m), covered with an air filter (Solberg F-15-050) and attached to a 30 m long ¼ inch Synflex 1300 Dekabon tubing (aluminium tape with an ethylene copolymer coating and an outer cover of high-density polyethylene) with an inner diameter of approximately 4.3 mm. Air samples are pressurized to 1.6 bar in 1 L glass flasks (Figure S2), with duplicates collected to minimize data loss, ensure quality control, and support uncertainty estimation. Prior to sample collection, the sampling tubing was flushed to remove residual air from the inlet system. Subsequently, air was directed through the sampling flasks, which were flushed with at least three times their internal volume. To avoid the influence of water vapor on greenhouse gas (GHG) mixing ratio measurements (Baier et al., 2020), the sampled air was dried using magnesium perchlorate before entering the flasks. Flasks are shipped from Colombia to the Max Planck Institute for Biogeochemistry (MPI-BGC) for analysis approximately every six months. Due to these logistical constraints, there is a substantial delay between sample collection and the availability of laboratory results. Experiments evaluating the effects of sample storage on atmospheric mixing ratios and isotopic composition have shown that storage does not substantially alter the measurements (Rothe et al., 2005). The transfer of samples from the measurement site to MPI-BGC results in an average lag of 238 days for greenhouse gas concentration measurements and 283 days for isotopic composition analyses (Figure S3). Since 13 May 2025, continuous wind speed and direction are measured at the top of the tower using a 1405-PK-165 Gill WindSonic® instrument.

2.2 Determination of surface influence or footprint

Spatially explicit surface influence maps (footprints) were calculated using the Stochastic Time Inverted Lagrangian Transport (STILT) model (Lin et al., 2003), following the setup of Botia et al. (Botía et al., 2022) for the Amazon Tall Tower Observatory. Back trajectories were computed by releasing 100 particles at each measurement coordinate (x, y, z, t), at the height of the flask inlet (z, 26 m). Gridded footprints were derived at a spatial resolution of 0.25° × 0.25° and defined as the flux sensitivity of mole fractions at the receptor location (units: ppm per µmol m^{-2} s^{-1}). From these, we computed: (1) the mean footprint over the full measurement period, with areas of influence corresponding to the 50th and 75th cumulative percentiles, and (2) monthly average footprints illustrating the seasonally varying surface influence over the 2023–2025 period.

https://doi.org/10.5194/essd-2026-831
Preprint. Discussion started: 9 November 2026
© Author(s) 2026. CC BY 4.0 License.



Open Access Earth System Science Data Discussions

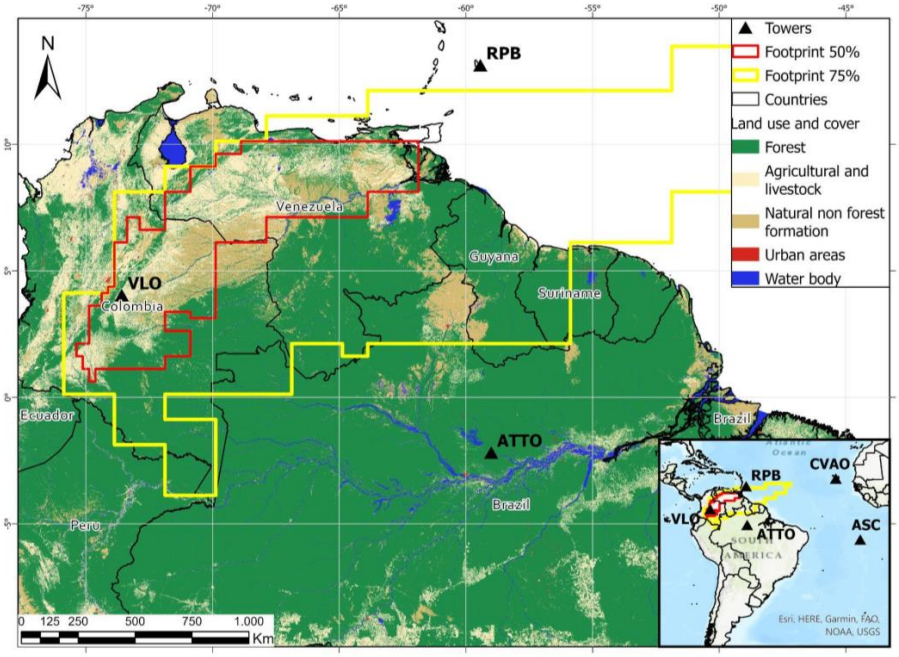


Figure 1. Map with the location of atmospheric monitoring towers across northern South American and the tropical Atlantic, including Amazon Tall Tower Observation (ATTO), Ragged Point Barbados (RPB), Ascension Island (ASC), Cape Verde Atmospheric Observatory (CVAO), and Villavicencio Tower (VLO) with red and yellow polygons that indicate the 50% and 75% cumulative footprints obtained using the STILT model (Lin et al., 2003). Monthly footprints can be observed in Figure 4. Land use and cover data for the year 2023 are based on MapBiomas, Collection 3 for Colombia and Venezuela, and Collection 6 for Amazonia. Sources: Esri, HERE, Garmin, FAO, NOAA, USGS | Powered by Esri.

2.3 Laboratory analysis

The atmospheric samples are analyzed for their GHG concentration and isotopic composition respectively in the Jena GasLab and IsoLab of the MPI-BGC. Gas Chromatography is used to measure the concentration of CO_2, CH_4, CO, N_2O, SF_6, H_2 in the samples. Mass spectrometry is used to analyze the isotopic composition of CO_2 (^{13}C and ^{18}O) and CH_4 (^{13}C and Deuterium), as well as O_2/N_2 and Ar/N_2. Table S1 gives an overview of the analytical methods and precision of each measurement. A detailed description of the analysis methods and instruments has been provided in Heimann et al. (Heimann et al., 2022). Uncertainties in the dataset are quantified by means of individual measurement uncertainty as provided by the laboratory, differences between duplicated samples and outlier detection (Figure 2 & 3).

2.4 Time series analysis

https://doi.org/10.5194/essd-2026-831
Preprint. Discussion started: 9 November 2026
© Author(s) 2026. CC BY 4.0 License.



In addition to the uncertainty provided by the Gas- and Iso-Labs, we identify statistical outliers in the flask time series by performing a two-stage procedure combining a robust spline fitting with iterative sigma-clipping based on the root-mean-square deviation (RMSD). For each species, a per-timestamp mean was first computed by averaging the upstream and downstream flask values. In the first stage, the spline was fitted to all duplicate means and the RMSD of the residuals was calculated. Any point whose residual exceeded three times the RMSD was removed, the spline was re-fitted to the remaining points, and the RMSD was recomputed. This process was repeated until no further points were rejected, yielding a robust spline that is not influenced by outliers. In the second stage, all original data points (i.e. the duplicate means) were evaluated against the final robust spline and a point was classified as an outlier if its residual exceeded three times the RMSD. The smoothing parameter of the cubic spline was set to $s = f \cdot n \cdot \sigma^2$, following the parameterisation of the UnivariateSpline function in the SciPy library (Virtanen et al., 2020) in python, where n is the number of data points and σ^2 is the sample variance. The species-specific scaling factor f was selected by visual inspection of the fitted spline for each species, balancing smoothness against the ability to capture real atmospheric variability (f = 0.35 for CH_4; f = 0.5 for CO_2, N_2O, CO, SF_6, and H_2; f = 0.7 for the isotope ratios, O_2/N_2 and Ar/N_2).

2.5 Data availability and format

The data are available in the following Zenodo repository: https://doi.org/10.5281/zenodo.23300649 and will be updated as new measurements become available. The current version (v1) covers the period June 2023 to March 2025. Data are provided as separate ASCII-formatted CSV files for each gas species or isotope measured. Each file starts with a short commented header containing metadata: station name, coordinates, sampling and ground altitude, time convention (UTC), flag definitions, dataset version and date, and the measured gas or isotope with its units. The header is followed by the observations, with one row per sampling date, giving the date and time (UTC), the mean mole fraction or isotopic value of the flask replicates, the standard deviation across replicates (σ), a quality flag indicating whether the value failed the time-series anomaly test, and the number of flasks averaged (N). Further details on the data format and processing are given in Heimann et al. (2022).

3. Results

The mole fraction time series of the different gases measured at the VLO tower are presented in Figure 2. The time series are characterized by temporally coherent measurements without any clear gaps, but with some outliers and discrepancies between duplicate samples detected for most gases (see also Figure S4). CO_2 shows an increase in mole fraction over time, with a clear seasonal pattern in which concentrations begin to decrease slightly from April–May and rise steeply around the end of the year (December–January). Methane mole fractions show a small but discernible increase over time, without a clear seasonal pattern, yet with mean mole fractions consistently above the global mean. N_2O shows a linear increase of approximately 3 ppb over the 21-month period analyzed here, with a similar trend observed in SF_6 mole fractions; however, SF_6 also exhibits a distinct seasonal pattern. CO displays a strong seasonal pattern, with peaks during February–April and, in 2024, an additional peak during August–September. Hydrogen exhibits an almost identical seasonal pattern to that of CO.

https://doi.org/10.5194/essd-2026-831
Preprint. Discussion started: 9 November 2026
© Author(s) 2026. CC BY 4.0 License.



Open Access Earth System Science Data Discussions

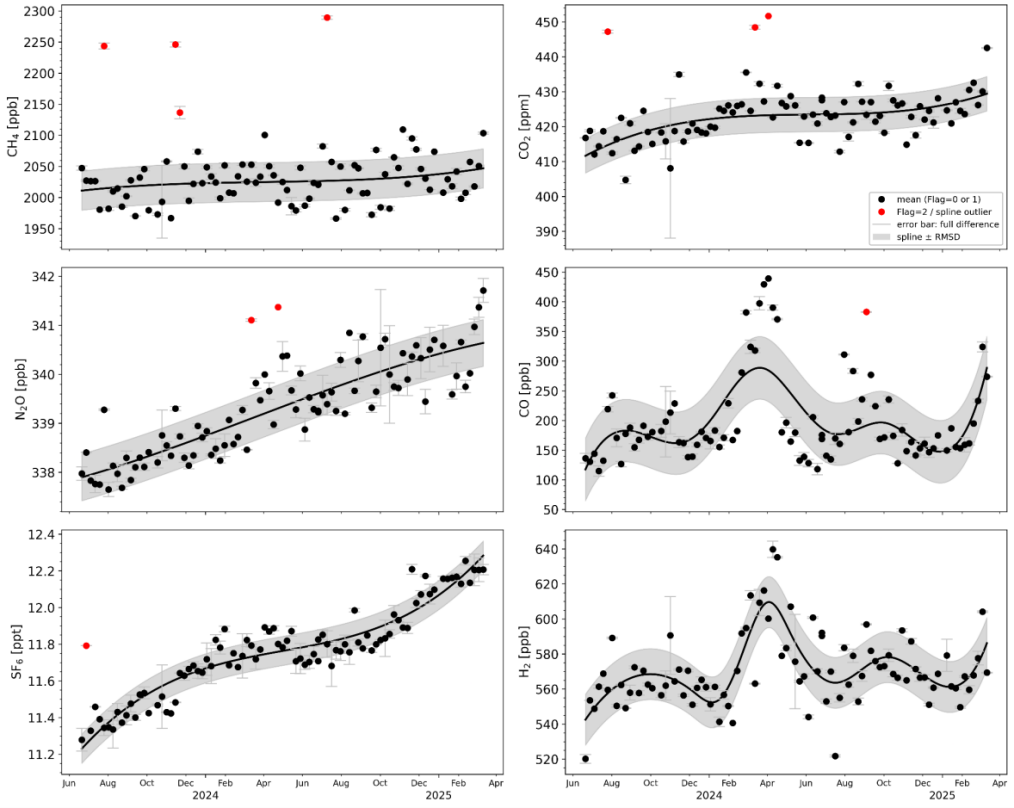


Figure 2. Time series of trace gas mole fractions measured from flask samples at station VLO (Universidad de los Llanos, Villavicencio, Colombia; 4.07°N, 73.58°W; 375 m a.s.l.). Dots indicate the mean value of the duplicate measurements, collected concurrently at 26 m above ground. The end of the whiskers represent the values of the individual flask measurements. Red markers indicate additional statistical outliers identified by iterative sigma-clipping of the spline residuals (rejection threshold: 3 × RMSD), applied only to data that passed the replicate criterion. Flagged points are excluded from the spline fit. All data are shown here for completeness, but individual studies may require the exclusion of samples that do not meet certain criteria. The same figure including all individual measurements is presented in Figure S4.

Results for the isotopic composition of CO_2 and CH_4, as well as O_2/N_2 and Ar/N_2 ratios, are presented in Figure 3. In line with the data presented in Figure 2, coherent time series with some outliers and excess replication differences are observed (see also figure S5). A decrease in $\delta^{13}C$ of CO_2 through time is observed, with more negative values during the dry season (January–May). No temporal trend in $\delta^{18}O$ of CO_2 is found; however, the same seasonal pattern is observed, with more negative values during the dry season. Time series of $\delta^{2}H$ and $\delta^{13}C$ of CH_4 show neither a clear temporal trend nor a seasonal pattern. O_2/N_2 ratios show a small decline over time, while no trend is observed in the Ar/N_2 ratios. Note that due to logistical constraints the time series of O_2/N_2 and Ar/N_2 started almost a month after all the other tracers.

https://doi.org/10.5194/essd-2026-831
Preprint. Discussion started: 9 November 2026
© Author(s) 2026. CC BY 4.0 License.

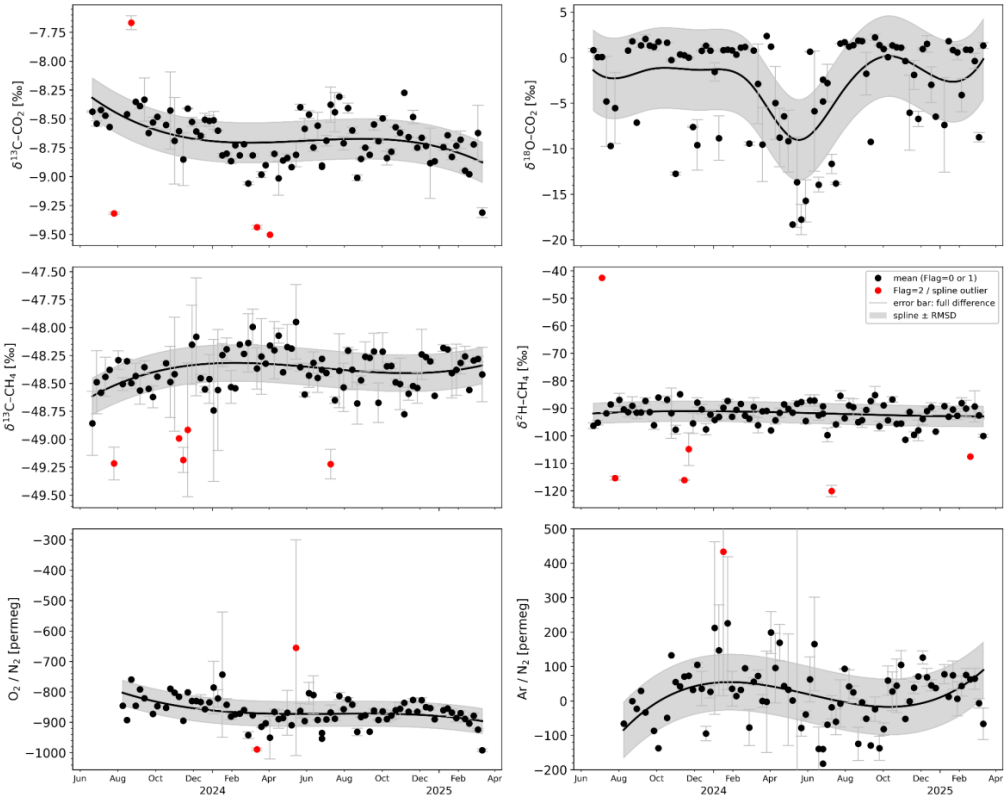


Figure 3. Time series of stable isotope ratios and atmospheric gas ratios at station VLO (Universidad de los Llanos, Villavicencio, Colombia; 4.07°N, 73.58°W; 375 m a.s.l.). Dots indicate the mean value of the duplicated samples, with the end of the whiskers representing the values of the individual flask measurements. Error bars denote measurement uncertainties. The solid black line is a robust cubic smoothing spline fitted to quality-controlled data; the grey band shows the spline ± RMSD. Red markers indicate sigma-clipping outliers. Flagged points are excluded from the spline fit. All data are shown here for completeness, but individual studies may require the exclusion of samples that do not meet certain criteria. The same figure including all individual measurements is presented in Figure S5.

4. Discussion

Here we present the first 21 months of atmospheric mixing ratios and stable isotopic composition measurements from the new atmospheric monitoring site in Villavicencio, Colombia (VLO). The time series collected up to date do not contain major long-term gaps and show overall good temporal consistency, although some spurious values and samples with large differences between duplicates were observed (Figures 2, 3 and S4, S5).

https://doi.org/10.5194/essd-2026-831
Preprint. Discussion started: 9 November 2026
© Author(s) 2026. CC BY 4.0 License.



We find that the mean annual footprint of the tower covers a large part of northern South America, with a particularly strong influence from the savannas of the Orinoco plains (Figure 1). However, this mean pattern masks important seasonal differences, which corresponds to the seasonality of most of the gases analyzed. Two main factors likely explain the observed seasonal variability in GHG mixing ratios and, to a lesser extent, in stable isotopic composition: (1) the footprint from which the atmospheric signal originates changes seasonally, and (2) the region is characterized by a well-defined dry season from December to April, which strongly affects biosphere-atmosphere gas exchange.

During the dry season (December–April), the footprint is dominated by the savannas of the Orinoco, whereas during the wetter months it shifts southward and becomes more strongly influenced by the northern Amazon forest region (Figure 4). Such a seasonal shift in footprint is expected to transport air masses originating from the Southern Hemisphere and passing over Amazonian forests, which have markedly different land-atmosphere exchange characteristics compared to the tropical savannas of the Orinoco plains. Consequently, this shift likely contributes substantially to the atmospheric signal measured at VLO.

The transition from predominantly Northern Hemisphere to Southern Hemisphere air masses can be clearly observed in the SF_6 time series. Atmospheric SF_6 concentrations are increasing nearly linearly at the global scale; however, because most emissions originate in the Northern Hemisphere, mixing ratios are systematically higher in the northern hemisphere than in the Southern Hemisphere. In our time series, we observe an initial linear increase in SF_6 concentrations, followed by a temporary stabilization when the footprint shifts southward, and finally a renewed increase when Northern Hemisphere air masses become dominant again from October onwards (Figures 2 & S4).

The second driver of the observed seasonal dynamics is the pronounced dry season that characterizes the region. Precipitation is generally very low during the December–April period, limiting photosynthesis and promoting widespread fires in the Orinoco savannas, as well as deforestation fires along the edge of the Amazon rainforest in Colombia (Arias et al., 2025). The influence of these fires is clearly visible in the CO time series, as CO is a tracer of incomplete combustion and is therefore strongly associated with wildfire occurrence (Figure 2). We observe a marked CO peak at the beginning of 2024 and the onset of another peak at the start of 2025. In agreement with the CO peak, we also observe elevated H_2 concentrations, higher CO_2 mixing ratios, and decreases in $\delta^{13}C$ and $\delta^{18}O$ in CO_2.

https://doi.org/10.5194/essd-2026-831
Preprint. Discussion started: 9 November 2026
© Author(s) 2026. CC BY 4.0 License.

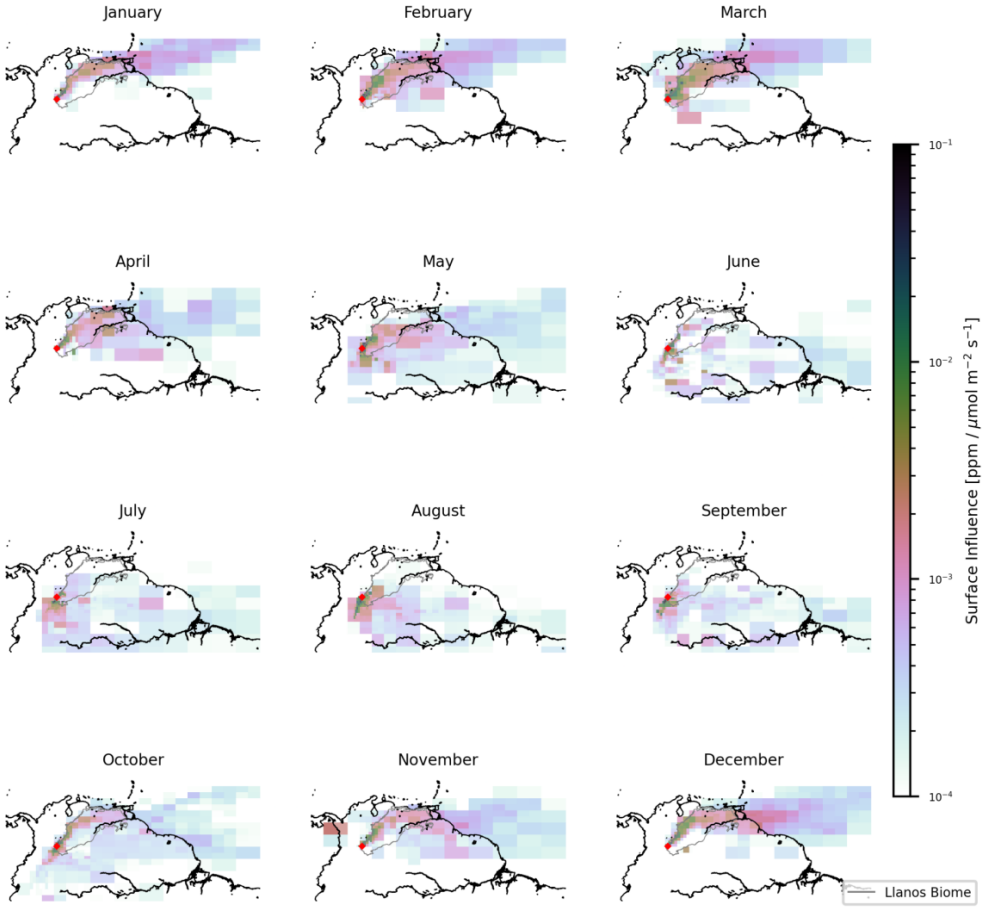


Figure 4. Monthly footprint for the Villavicencio Tower (VLO) at Universidad de los Llanos (4.073, -73.584) simulated at 26 m height. For the simulation we used the STILT model (Lin et al., 2003). The model was run for all times in which there are flasks data available (June 2023 to March 2025).

VLO is located relatively close to the Andean foothills, where the pronounced topographic gradient influences local wind patterns (Figure S6). This influence is especially noticeable from the evening until the early morning, when wind direction is dominated by westerly winds originating from the mountainous region. During daytime, the prevailing wind direction shifts and becomes aligned with the dominant regional easterly circulation. Consequently, the flask measurements which are conducted between 12-2pm predominantly sample air bringing signals from the targeted regions to the east. However, because the city of Villavicencio is located only 9 km west of the tower, the atmospheric composition measured at the site can be affected by the urban plume during the relatively infrequent periods when winds originate from westerly directions.

While we present here only the first 21 months of data collected at the tower, corresponding to the dataset available at the time of writing this manuscript, measurements have continued without interruption up to now. Once a sufficiently long time series has been established, the VLO observations are expected to be incorporated into the Jena CarboScope inversion framework for

https://doi.org/10.5194/essd-2026-831
Preprint. Discussion started: 9 November 2026
© Author(s) 2026. CC BY 4.0 License.



CH_4 and CO_2. The VLO station is envisioned as a long-term atmospheric monitoring site for northern South America, and we anticipate continuing the sampling into the foreseeable future. We expect to share the data with the community for evaluating regional and global atmospheric transport inversions.

5. Conclusions

Atmospheric measurements have been conducted continuously at the Villavicencio Tower (VLO) since 20 June 2023. The current time series does not contain any major gaps and shows overall good temporal consistency, with only a limited number of anomalous values or samples exhibiting large differences between replicates. The footprint of VLO covers large parts of northern South America, a region that is currently not represented by any other atmospheric monitoring station. As such, VLO provides a unique observational dataset for monitoring atmospheric composition and improving our understanding of biosphere–atmosphere interactions in this key tropical region. As the observational record continues to expand, the VLO dataset is expected to contribute to regional and global atmospheric inversion frameworks and to help reduce current uncertainties in greenhouse gas sources and sinks across northern South America.

Data availability

The dataset presented here is stored at the Zenodo repository: https://doi.org/10.5281/zenodo.23300649 (Hantson et al., 2026)

Author contribution

SH - Conceptual design, writing manuscript, data analysis
SB - Conceptual design, writing manuscript, data analysis
MANR - Conceptual design, weekly sampling
DPB - weekly sampling
JFA - technical support, weekly sampling
SW - data analysis
MARN - weekly sampling
AG - data analysis
MS - data analysis
MH - data analysis (flagging routine of MPI-BGC network)
AJ - Trace gas analysis
SK - Trace gas analysis
HM - Isotope Lab Analysis
MR - Isotope Lab Analysis
CR - data analysis (flagging routine of MPI-BGC network)
SZ - writing manuscript
CS - Conceptual design, writing manuscript

SH and SB wrote the manuscript with contributions from all coauthors.

https://doi.org/10.5194/essd-2026-831
Preprint. Discussion started: 9 November 2026
© Author(s) 2026. CC BY 4.0 License.



Competing interests

The authors declare they have no competing interests.

Acknowledgment

SH acknowledges support from the Max Planck Tandem Group program of the Max Planck Society. SH acknowledges support from Universidad del Rosario within the program of Capital Semilla. SH acknowledges support from the Ministry of Sciences of Colombia (Contract 455-2023). SB acknowledges the support from the former BMBF (Bundesministerium für Bildung und Forschung) now renamed to BMFTR (Bundesministerium für Forschung, Technologie und Raumfahrt) that funded the C2SAV Project under the contract 01DN24003 in the context of the call B-AMERIKA Forderaufruf Wissenschaftlich-Technologische Zusammenarbeit mit Kolumbien. We want to thank Laurentino Matta for his support with the organization and logistics of the flask measurements. The authors used AI-assisted tools for language editing and grammatical correction. The article processing charges for this open-access publication were covered by the Max Planck Society.

https://doi.org/10.5194/essd-2026-831
Preprint. Discussion started: 9 November 2026
© Author(s) 2026. CC BY 4.0 License.



Bibliography

Andreae, M. O., Acevedo, O. C., Araùjo, A., Artaxo, P., Barbosa, C. G. G., Barbosa, H. M. J., Brito, J., Carbone, S., Chi, X., Cintra, B. B. L., da Silva, N. F., Dias, N. L., Dias-Júnior, C. Q., Ditas, F., Ditz, R., Godoi, A. F. L., Godoi, R. H. M., Heimann, M., Hoffmann, T., Kesselmeier, J., Könemann, T., Krüger, M. L., Lavric, J. V., Manzi, A. O., Lopes, A. P., Martins, D. L., Mikhailov, E. F., Moran-Zuloaga, D., Nelson, B. W., Nölscher, A. C., Santos Nogueira, D., Piedade, M. T. F., Pöhlker, C., Pöschl, U., Quesada, C. A., Rizzo, L. V., Ro, C.-U., Ruckteschler, N., Sá, L. D. A., de Oliveira Sá, M., Sales, C. B., dos Santos, R. M. N., Saturno, J., Schöngart, J., Sörgel, M., de Souza, C. M., de Souza, R. A. F., Su, H., Targhetta, N., Tóta, J., Trebs, I., Trumbore, S., van Eijck, A., Walter, D., Wang, Z., Weber, B., Williams, J., Winderlich, J., Wittmann, F., Wolff, S., and Yáñez-Serrano, A. M.: The Amazon Tall Tower Observatory (ATTO): overview of pilot measurements on ecosystem ecology, meteorology, trace gases, and aerosols, Atmospheric Chem. Phys., 15, 10723–10776, https://doi.org/10.5194/acp-15-10723-2015, 2015.

Arias, P., Bellouin, N., Coppola, E., Jones, R., Krinner, G., Marotzke, J., Naik, V., Palmer, M., Plattner, G.-K., and Rogelj, J.: Climate Change 2021: the physical science basis. Contribution of Working Group I to the Sixth Assessment Report of the Intergovernmental Panel on Climate Change; technical summary, https://doi.org/10.1017/9781009157896.002, 2021.

Arias, P. A., Fernández-Berrío, A., Bedoya-Pineda, V., Acevedo-Ortiz, M. Y., and Martínez, J. A.: Compound dry and hot extremes and their implications for fire activity over the Orinoco River Basin in northern South America, Clim. Dyn., 63, 175, https://doi.org/10.1007/s00382-025-07660-5, 2025.

Baier, B. C., Sweeney, C., Choi, Y., Davis, K. J., DiGangi, J. P., Feng, S., Fried, A., Halliday, H., Higgs, J., Lauvaux, T., Miller, B. R., Montzka, S. A., Newberger, T., Nowak, J. B., Patra, P., Richter, D., Walega, J., and Weibring, P.: Multispecies Assessment of Factors Influencing Regional CO2 and CH4 Enhancements During the Winter 2017 ACT-America Campaign, J. Geophys. Res. Atmospheres, 125, e2019JD031339, https://doi.org/10.1029/2019JD031339, 2020.

Botía, S., Komiya, S., Marshall, J., Koch, T., Gałkowski, M., Lavric, J., Gomes-Alves, E., Walter, D., Fisch, G., Pinho, D. M., Nelson, B. W., Martins, G., Luijkx, I. T., Koren, G., Florentie, L., Carioca de Araújo, A., Sá, M., Andreae, M. O., Heimann, M., Peters, W., and Gerbig, C.: The CO2 record at the Amazon Tall Tower Observatory: A new opportunity to study processes on seasonal and inter-annual scales, Glob. Change Biol., 28, 588–611, https://doi.org/10.1111/gcb.15905, 2022.

Botía, S., Munassar, S., Koch, T., Custodio, D., Basso, L. S., Komiya, S., Lavric, J. V., Walter, D., Gloor, M., Martins, G., Naus, S., Koren, G., Luijkx, I. T., Hantson, S., Miller, J. B., Peters, W., Rödenbeck, C., and Gerbig, C.: Combined CO2 measurement record indicates Amazon forest carbon uptake is offset by savanna carbon release, Atmos Chem Phys, 25, 6219–6255, https://doi.org/10.5194/acp-25-6219-2025, 2025.

Buchwitz, M., Reuter, M., Schneising, O., Boesch, H., Guerlet, S., Dils, B., Aben, I., Armante, R., Bergamaschi, P., Blumenstock, T., Bovensmann, H., Brunner, D., Buchmann, B., Burrows, J. P., Butz, A., Chédin, A., Chevallier, F., Crevoisier, C. D., Deutscher, N. M., Frankenberg, C., Hase, F., Hasekamp, O. P., Heymann, J., Kaminski, T., Laeng, A., Lichtenberg, G., Mazière, M. D., Noël, S., Notholt, J., Orphal, J., Popp, C., Parker, R., Scholze, M., Sussmann, R., Stiller, G. P., Warneke, T., Zehner, C., Bril, A., Crisp, D., Griffith, D. W. T., Kuze, A., O'Dell, C., Oshchepkov, S., Sherlock, V., Suto, H., Wennberg, P., Wunch, D., Yokota, T., and Yoshida, Y.: The Greenhouse Gas Climate Change Initiative (GHG-CCI):

https://doi.org/10.5194/essd-2026-831
Preprint. Discussion started: 9 November 2026
© Author(s) 2026. CC BY 4.0 License.



464 Comparison and quality assessment of near-surface-sensitive satellite-derived CO2 and CH4 global
465 data sets, Remote Sens. Environ., 162, 344–362,
466 https://doi.org/https://doi.org/10.1016/j.rse.2013.04.024, 2015.

467 Canadell, J. G., Monteiro, P. M., Costa, M. H., Da Cunha, L. C., Cox, P. M., Eliseev, A. V., Henson, S.,
468 Ishii, M., Jaccard, S., and Koven, C.: Global carbon and other biogeochemical cycles and feedbacks,
469 IPCC AR6 WGI Final Gov. Distrib., chapter-5, https://doi.org/10.1017/9781009157896.007, 2021.

470 Ciais, P., Sabine, C., Bala, G., Bopp, L., Brovkin, V., Canadell, J., Chhabra, A., DeFries, R., Galloway, J.,
471 and Heimann, M.: Climate change 2013: the physical science basis, Contrib. Work. Group Fifth
472 Assess. Rep. Intergov. Panel Clim. Change Chapter Carbon Biogeochem. Cycles Camb. Univ. Press
473 Camb., https://doi.org/10.1017/CBO9781107415324.015, 2013.

474 Feng, L., Palmer, P. I., Zhu, S., Parker, R. J., and Liu, Y.: Tropical methane emissions explain large
475 fraction of recent changes in global atmospheric methane growth rate, Nat. Commun., 13, 1378,
476 https://doi.org/10.1038/s41467-022-28989-z, 2022.

477 Fernandes Amaral, J. H., Botía, S., Torres Quintero, P., Gutierrez Rincon, A. S., Ho, D., Sanchez, A.,
478 Avila-Diaz, A., Uhde, A., Quesada, B., Benavides, J. C., Winton, R. S., Sierra, C. A., Navarro-Ramírez,
479 M. A., Pardo Buitrago, D. D., and Hantson, S.: Methane fluxes from tropical wetlands of the Orinoco
480 River Basin and their regional implications, EGUsphere, 2026, 1–34,
481 https://doi.org/10.5194/egusphere-2026-2080, 2026.

482 France, J. L., Lunt, M. F., Andrade, M., Moreno, I., Ganesan, A. L., Lachlan-Cope, T., Fisher, R. E.,
483 Lowry, D., Parker, R. J., Nisbet, E. G., and Jones, A. E.: Very large fluxes of methane measured above
484 Bolivian seasonal wetlands, Proc. Natl. Acad. Sci., 119, e2206345119,
485 https://doi.org/10.1073/pnas.2206345119, 2022.

486 Frankenberg, C., Bar-On, Y. M., Yin, Y., Wennberg, P. O., Jacob, D. J., and Michalak, A. M.: Data
487 Drought in the Humid Tropics: How to Overcome the Cloud Barrier in Greenhouse Gas Remote
488 Sensing, Geophys. Res. Lett., 51, e2024GL108791,
489 https://doi.org/https://doi.org/10.1029/2024GL108791, 2024.

490 Friedlingstein, P., O'Sullivan, M., Jones, M. W., Andrew, R. M., Bakker, D. C. E., Hauck, J.,
491 Landschützer, P., Le Quéré, C., Li, H., Luijkx, I. T., Peters, G. P., Peters, W., Pongratz, J., Schwingshackl,
492 C., Sitch, S., Canadell, J. G., Ciais, P., Aas, K., Alin, S. R., Anthoni, P., Barbero, L., Bates, N. R., Bellouin,
493 N., Benoit-Cattin, A., Berghoff, C. F., Bernardello, R., Bopp, L., Brasika, I. B. M., Chamberlain, M. A.,
494 Chandra, N., Chevallier, F., Chini, L. P., Collier, N. O., Colligan, T. H., Cronin, M., Djeutchouang, L.,
495 Dou, X., Enright, M. P., Enyo, K., Erb, M., Evans, W., Feely, R. A., Feng, L., Ford, D. J., Foster, A.,
496 Fransner, F., Gasser, T., Gehlen, M., Gkritzalis, T., Goncalves De Souza, J., Grassi, G., Gregor, L.,
497 Gruber, N., Guenet, B., Gürses, Ö., Harrington, K., Harris, I., Heinke, J., Hurtt, G. C., Iida, Y., Ilyina, T.,
498 Ito, A., Jacobson, A. R., Jain, A. K., Jarníková, T., Jersild, A., Jiang, F., Jones, S. D., Kato, E., Keeling, R.
499 F., Klein Goldewijk, K., Knauer, J., Kong, Y., Korsbakken, J. I., Koven, C., Kunimitsu, T., Lan, X., Liu, J.,
500 Liu, Z., Liu, Z., Lo Monaco, C., Ma, L., Marland, G., McGuire, P. C., McKinley, G. A., Melton, J., Monacci,
501 N., Monier, E., Morgan, E. J., Munro, D. R., Müller, J. D., Nakaoka, S.-I., Nayagam, L. R., Niwa, Y.,
502 Nutzel, T., Olsen, A., Omar, A. M., Pan, N., Pandey, S., et al.: Global Carbon Budget 2025,
503 https://doi.org/10.5194/essd-2025-659, 13 November 2025.

https://doi.org/10.5194/essd-2026-831
Preprint. Discussion started: 9 November 2026
© Author(s) 2026. CC BY 4.0 License.



504 Gatti, L. V., Basso, L. S., Miller, J. B., Gloor, M., Gatti Domingues, L., Cassol, H. L. G., Tejada, G.,
505 Aragão, L. E. O. C., Nobre, C., Peters, W., Marani, L., Arai, E., Sanches, A. H., Corrêa, S. M., Anderson,
506 L., Von Randow, C., Correia, C. S. C., Crispim, S. P., and Neves, R. A. L.: Amazonia as a carbon source
507 linked to deforestation and climate change, Nature, 595, 388–393, https://doi.org/10.1038/s41586-
508 021-03629-6, 2021.

509 Gatti, L. V., Cunha, C. L., Marani, L., Cassol, H. L. G., Messias, C. G., Arai, E., Denning, A. S., Soler, L.
510 S., Almeida, C., Setzer, A., Domingues, L. G., Basso, L. S., Miller, J. B., Gloor, M., Correia, C. S. C.,
511 Tejada, G., Neves, R. A. L., Rajao, R., Nunes, F., Filho, B. S. S., Schmitt, J., Nobre, C., Corrêa, S. M.,
512 Sanches, A. H., Aragão, L. E. O. C., Anderson, L., Von Randow, C., Crispim, S. P., Silva, F. M., and
513 Machado, G. B. M.: Increased Amazon carbon emissions mainly from decline in law enforcement,
514 Nature, 621, 318–323, https://doi.org/10.1038/s41586-023-06390-0, 2023.

515 Gentine, P., Massmann, A., Lintner, B. R., Hamed Alemohammad, S., Fu, R., Green, J. K., Kennedy,
516 D., and Vilà-Guerau de Arellano, J.: Land–atmosphere interactions in the tropics – a review, Hydrol.
517 Earth Syst. Sci., 23, 4171–4197, https://doi.org/10.5194/hess-23-4171-2019, 2019.

518 Gloor, M., Gatti, L. V., Wilson, C., Parker, R. J., Boesch, H., Popa, E., Chipperfield, M. P., Poulter, B.,
519 Zhang, Z., Basso, L., Miller, J., McNorton, J., Jimenez, C., and Prigent, C.: Large Methane Emissions
520 From the Pantanal During Rising Water-Levels Revealed by Regularly Measured Lower Troposphere
521 CH4 Profiles, Glob. Biogeochem. Cycles, 35, e2021GB006964,
522 https://doi.org/https://doi.org/10.1029/2021GB006964, 2021.

523 Hancock, S. E., Jacob, D. J., Chen, Z., Nesser, H., Davitt, A., Varon, D. J., Sulprizio, M. P., Balasus, N.,
524 Estrada, L. A., Cazorla, M., Dawidowski, L., Diez, S., East, J. D., Penn, E., Randles, C. A., Worden, J.,
525 Aben, I., Parker, R. J., and Maasakkers, J. D.: Satellite quantification of methane emissions from
526 South American countries: a high-resolution inversion of TROPOMI and GOSAT observations,
527 Atmospheric Chem. Phys., 25, 797–817, https://doi.org/10.5194/acp-25-797-2025, 2025.

528 Hancock, S. E., Jacob, D. J., Jimenez, R., Ardila, A., Morales-Rincon, L., Rojas, N., Estrada, L. A.,
529 Balasus, N., East, J. D., Sulprizio, M. P., Wang, X., France, J. L., Potyk, L., Penn, E., Chen, Z., Varon, D.
530 J., Frankenberg, C., Baranski, M., Calcan, A., and Parker, R. J.: Applying Satellite Observations to
531 Improve Bottom-Up National Emission Inventories for Methane: Application to Colombia,
532 EGUsphere, 2026, 1–29, https://doi.org/10.5194/egusphere-2025-5478, 2026.

533 Hantson, S., Botía, S., Navarro-Ramírez, M. Á., Pardo-Buitrago, D., Fernandes Amaral, J., Wagh, S.,
534 Ramírez-Niño, M. Á., Gutiérrez-Rincón, A., Salamanca-Fonseca, M., Jordan, A., Knabe, S., El Madany,
535 T., Kübler, K., Moossen, H., Rothe, M., Rödenbeck, C., & Sierra, C. (2026). High precision atmospheric
536 GHG and stable isotope measurements at The Villavicencio Tower (VLO) [Dataset].
537 Zenodo. https://doi.org/10.5281/zenodo.23300649

538 He, M., Jacob, D. J., Estrada, L. A., Varon, D. J., Sulprizio, M., Balasus, N., East, J. D., Penn, E.,
539 Pendergrass, D. C., Chen, Z., Mooring, T. A., Maasakkers, J. D., Brodrick, P. G., Frankenberg, C.,
540 Bowman, K. W., and Bruhwiler, L.: Attributing 2019–2024 methane growth using TROPOMI satellite
541 observations, Sci. Adv., 12, eadz9007, https://doi.org/10.1126/sciadv.adz9007, 2026.

542 Heimann, M., Jordan, A., Brand, W., Lavrič, J., Moossen, H., and Rothe, M.: The atmospheric flask
543 sampling program of MPI-BGC Version 13, 2022, https://doi.org/10.17617/3.8r, 2022.

https://doi.org/10.5194/essd-2026-831
Preprint. Discussion started: 9 November 2026
© Author(s) 2026. CC BY 4.0 License.



544 Houweling, S., Bergamaschi, P., Chevallier, F., Heimann, M., Kaminski, T., Krol, M., Michalak, A. M.,
545 and Patra, P.: Global inverse modeling of CH_4 sources and sinks:\hack\newline an overview of
546 methods, Atmospheric Chem. Phys., 17, 235–256, https://doi.org/10.5194/acp-17-235-2017, 2017.

547 Lin, J. C., Gerbig, C., Wofsy, S. C., Andrews, A. E., Daube, B. C., Davis, K. J., and Grainger, C. A.: A near-
548 field tool for simulating the upstream influence of atmospheric observations: The Stochastic Time-
549 Inverted Lagrangian Transport (STILT) model, J. Geophys. Res. Atmospheres, 108,
550 https://doi.org/10.1029/2002JD003161, 2003.

551 Peylin, P., Law, R., Gurney, K., Chevallier, F., Jacobson, A., Maki, T., Niwa, Y., Patra, P., Peters, W.,
552 and Rayner, P.: Global atmospheric carbon budget: results from an ensemble of atmospheric CO2
553 inversions, Biogeosciences, 10, 6699–6720, https://doi.org/10.5194/bg-10-6699-2013, 2013.

554 Rothe, M., Jordan, A., and Brand, W. A.: Trace gases, δ13C and δ18O of CO2-in-air samples: Storage
555 in glass flasks using PCTFE seals and other effects, in: Proceedings of the 12th IAEA/WMO meeting
556 of CO2 experts, Toronto, Sept. 2003, edited by: Worthy, D. and Huang, L., 64–70, 2005.
557 https://hdl.handle.net/11858/00-001M-0000-000E-D36E-0

558 Saunois, M., Martinez, A., Poulter, B., Zhang, Z., Raymond, P. A., Regnier, P., Canadell, J. G., Jackson,
559 R. B., Patra, P. K., and Bousquet, P.: Global methane budget 2000–2020, Earth Syst. Sci. Data, 17,
560 1873–1958, https://doi.org/10.5194/essd-17-1873-2025, 2025.

561 Schuldt, K. N., Mund, J., Aalto, T., Aaltonen, H., Abshire, J. B., Aikin, K., Allen, G., Andrade, M.,
562 Apadula, F., Arnold, S., Baier, B., Bakwin, P., Bäni, L., Bartyzel, J., Bentz, G., Bergamaschi, P.,
563 Beyersdorf, A., Biermann, T., Biraud, S. C., Pierre-Eric Blanc, Boenisch, H., Bowling, D., Brailsford, G.,
564 Brand, W. A., Brunner, D., Bui, T. P. V., van den Bulk, P., Benoit Burban, Francescopiero Calzolari,
565 Chang, C. S., Chen, G., Huilin Chen, Lukasz Chmura, St. Clair, J. M., Clark, S., Sites Climadat, Coletta,
566 J. D., Colomb, A., Commane, R., Condori, L., Conen, F., Conil, S., Couret, C., Cristofanelli, P., Cuevas,
567 E., Curcoll, R., Daube, B., Davis, K. J., Dean-Day, J. M., Delmotte, M., Dickerson, R., DiGangi, E.,
568 DiGangi, J. P., Elsasser, M., Emmenegger, L., Shuangxi Fang, Forster, G., France, J., Frumau, A.,
569 Fuente-Lastra, M., Galkowski, M., Gatti, L. V., Gehrlein, T., Gerbig, C., Francois Gheusi, Gloor, E.,
570 Goto, D., Griffis, T., Hammer, S., Hanisco, T. F., Hanson, C., Hashimoto, S., Haszpra, L., Hatakka, J.,
571 Heimann, M., Heliasz, M., Heltai, D., Henne, S., Hensen, A., Hermans, C., Hermansen, O., Higgs, J.,
572 Hintsa, E., Hoheisel, A., Holst, J., Di Iorio, T., Iraci, L. T., Ivakhov, V., Jaffe, D. A., Joly, L., Jordan, A.,
573 Joubert, W., Kang, H.-Y., Karion, A., Kawa, S. R., Kazan, V., Keeling, R. F., Ishijima Kentaro, Keronen,
574 P., et al.: Multi-laboratory compilation of atmospheric carbon dioxide data for the period 1957-
575 2024; obspack_co2_1_GLOBALVIEWplus_v11.0_2026-01-12, https://doi.org/10.25925/20250801,
576 2025.

577 Sierra, C. A., Chanca, I., Andreae, M. O., de Araújo, A. C., van Asperen, H., Borchardt, L., Botía, S.,
578 Candido, L. A., Correa, C. S. C., Dias-Junior, C. Q., Eritt, M., Fröhlich, A., Gatti, L. V., Guderle, M.,
579 Hammer, S., Heimann, M., Horna, V., Jordan, A., Knabe, S., Kneißl, R., Lavric, J. V., Levin, I., Macario,
580 K., Menger, J., Moossen, H., Quesada, C. A., Rothe, M., Rödenbeck, C., Santos, Y., Steinhof, A.,
581 Takeshi, B., Trumbore, S., and Zaehle, S.: The flask monitoring program for high-precision
582 atmospheric measurements of greenhouse gases, stable isotopes, and radiocarbon in the central
583 Amazon region, Earth Syst. Sci. Data, 17, 5871–5884, https://doi.org/10.5194/essd-17-5871-2025,
584 2025.

https://doi.org/10.5194/essd-2026-831
Preprint. Discussion started: 9 November 2026
© Author(s) 2026. CC BY 4.0 License.



585 Tian, H., Pan, N., Thompson, R. L., Canadell, J. G., Suntharalingam, P., Regnier, P., Davidson, E. A.,
586 Prather, M., Ciais, P., and Muntean, M.: Global nitrous oxide budget (1980–2020), Earth Syst. Sci.
587 Data, 16, 2543–2604, https://doi.org/10.5194/essd-16-2543-2024, 2024.

588 Virtanen, P., Gommers, R., Oliphant, T. E., Haberland, M., Reddy, T., Cournapeau, D., Burovski, E.,
589 Peterson, P., Weckesser, W., Bright, J., van der Walt, S. J., Brett, M., Wilson, J., Millman, K. J.,
590 Mayorov, N., Nelson, A. R. J., Jones, E., Kern, R., Larson, E., Carey, C. J., Polat, İ., Feng, Y., Moore, E.
591 W., VanderPlas, J., Laxalde, D., Perktold, J., Cimrman, R., Henriksen, I., Quintero, E. A., Harris, C. R.,
592 Archibald, A. M., Ribeiro, A. H., Pedregosa, F., van Mulbregt, P., Vijaykumar, A., Bardelli, A. P.,
593 Rothberg, A., Hilboll, A., Kloeckner, A., Scopatz, A., Lee, A., Rokem, A., Woods, C. N., Fulton, C.,
594 Masson, C., Häggström, C., Fitzgerald, C., Nicholson, D. A., Hagen, D. R., Pasechnik, D. V., Olivetti, E.,
595 Martin, E., Wieser, E., Silva, F., Lenders, F., Wilhelm, F., Young, G., Price, G. A., Ingold, G.-L., Allen, G.
596 E., Lee, G. R., Audren, H., Probst, I., Dietrich, J. P., Silterra, J., Webber, J. T., Slavič, J., Nothman, J.,
597 Buchner, J., Kulick, J., Schönberger, J. L., de Miranda Cardoso, J. V., Reimer, J., Harrington, J.,
598 Rodríguez, J. L. C., Nunez-Iglesias, J., Kuczynski, J., Tritz, K., Thoma, M., Newville, M., Kümmerer, M.,
599 Bolingbroke, M., Tartre, M., Pak, M., Smith, N. J., Nowaczyk, N., Shebanov, N., Pavlyk, O., Brodtkorb,
600 P. A., Lee, P., McGibbon, R. T., Feldbauer, R., Lewis, S., Tygier, S., Sievert, S., Vigna, S., Peterson, S.,
601 More, S., Pudlik, T., et al.: SciPy 1.0: fundamental algorithms for scientific computing in Python, Nat.
602 Methods, 17, 261–272, https://doi.org/10.1038/s41592-019-0686-2, 2020.

603 Watts, J. D., Ordway, E., Malone, S. L., Zhu, Q., Palmer, P. I., Patel-Tupper, D., Ciais, P., Li, F.,
604 Monteverde, D. R., Arndt, K. A., Bruhwiler, L., Buma, B., Cadillo-Quiroz, H., Euskirchen, E., Hoyt, A.
605 M., Holgerson, M., Hugelius, G., Jackson, R. B., Jacob, D., Kuhn, M., Natali, S. M., Peng, S., Perryman,
606 C. R., Poulter, B., Rey-Sánchez, C., Sagang, L. B., Schuur, E. A. G., Varner, R. K., and Vargas, R.: A global
607 methane observation system to track climate feedbacks for verifiable climate impact, Science, 391,
608 1324–1327, https://doi.org/10.1126/science.aef0459, 2026.